Annals of Nuclear Energy 99 (2017) 484–494

Contents lists available at ScienceDirect

Annals of Nuclear Energy

journal homepage: www.elsevier.com/locate/anucene

Simulation of a sodium fast core: Effect of B_1 leakage models on group constant generation

B. Faure *, G. Marleau

Institut de Génie Nucléaire, École Polytechnique de Montréal, Montréal, Québec H3C 3A7, Canada

ARTICLE INFO

Article history:
Received 29 July 2016
Received in revised form 29 September 2016
Accepted 4 October 2016
Available online 18 October 2016

Keywords:
Neutron transport and diffusion
Lattice calculation
Leakage models
Sodium fast reactor

ABSTRACT

Due to their complexity, neutronic calculations are usually performed in two steps. Once the neutron transport equation has been solved over the elementary domains that compose the core (cells or assemblies with translation or reflexion boundary conditions), a set of parameters – namely macroscopic cross sections and potentially diffusion coefficients – are generated in order to model the whole core as a simplified problem which is often treated in diffusion theory.

The first calculation being over a periodic lattice of cells or assemblies, leakage between different domains of the core and out of the lattice needs to be explicitly taken into account by an additional term that must be added in the neutron transport equation. For historical reasons, the leakage term is in most cases modeled by a homogeneous and isotropic probability within a "homogeneous leakage model" that is compatible with the classical collision probability method often used to solve the neutron transport equation. Driven by technological innovation in the field of computer science, "heterogeneous leakage models" have been developed and implemented in several neutron transport calculation codes.

The present work discusses the effect of the leakage model used for the generation of diffusion parameters on sodium fast reactor diffusion calculations. Homogenized and condensed cross sections as well as diffusion coefficients are calculated for hexagonal sodium fast reactor assemblies using the lattice code DRAGON-3. Three different calculations are performed for each assembly: without taking neutron leakage into account, using the classical homogeneous B_1 procedure or with the heterogeneous B_1 TIBERE model. Furthermore, a homogeneous core and a simple heterogeneous core are calculated within diffusion theory using the DONJON-5 code and the results are compared with a Monte Carlo calculation.

It is shown that, even if a fissile assembly can be calculated without leakage, the heterogeneous TIBERE model is best suited for "cluster calculations" (a fertile or reflector assembly surrounded by fuel assemblies). Moreover, the homogeneous B_1 model should be avoided in such calculations since it is not able to handle streaming effects between the different assemblies.

1. Introduction

The neutronic calculation of reactor cores consists in solving the Boltzmann transport equation for the neutron flux over a specific geometry. For practical purposes, the case of an infinite lattice is often considered by modeling a heterogeneous cell or assembly with translation or reflexion boundary conditions. Because of this representation, a "leakage model" is needed if effects such as neutron streaming between zones of different composition in the real core or leakage out of the physical domain are to be explicitly taken into account. Treating these phenomena correctly is a problem of primary importance since neutron streaming is likely to have an impact on the energy distribution of the neutrons over the geometry and therefore on the homogenized and condensed cross sections needed for whole core calculations. Besides, if that last step is to be performed within diffusion theory, which is often the case, the correct evaluation of neutron streaming is desirable since it is tightly linked to the definition of the diffusion coefficient.

Leakage models consist in adding an additional term in the neutron transport equation and in defining an algorithmic procedure for achieving criticality within the infinite lattice, such state being representative of the reactor normal operating conditions. The historical choice of the collision probability method to solve the transport equation being limited to an isotropic distribution for the neutronic sources, it has influenced the derivation of a "homogeneous leakage model" that proposes to replace the leakage term by the uniform and isotropic probability that arises in a homogeneous media. Still used in many practical calculations,

* Corresponding author.
E-mail addresses: bastien.faure@polymtl.ca (B. Faure), guy.marleau@polymtl.ca (G. Marleau).

http://dx.doi.org/10.1016/j.anucene.2016.10.002
0306-4549/

the homogeneous leakage model now faces other more refined "heterogeneous models" that have become very competitive given the progress that has been made in the field of computer science.

The origins of such heterogeneous models may be found in Behrens (1949) where the impact of holes on the migration area of neutrons is studied. From this point on, the effect of heterogeneity has been widely explored in order to elaborate models that could take correctly into account neutron streaming. For instance, several studies have been carried out by Leslie (1962), Larsen (1975), Kohler (1975) or Bonalumi (1981) arising in many practical definitions for the diffusion coefficient. Together with a general formalism for the leakage model, a review of those definitions has been proposed by Gelbard (1983) and Deniz (1986). In Benoist's theory (Benoist, 1961, 1984, 1986, Petrovic and Benoist (1997)), a model capable of handling heterogeneous and anisotropic streaming is derived for the collision probability method, leading to the definition of directional diffusion coefficients. Known as the TIBERE model, it is used in neutron transport codes such as APOLLO-2 or DRAGON-3. A simplified form of this model has been implemented in the ECCO cell code (Rimpault, 1997) and then generalized to other types of solution of the transport equation in Hébert (2009). Recently, Van-Rooijen and Chiba (2011) have used the method of characteristics to solve the exact neutron leakage problem, applying it with success to the hexagonal cell of a sodium fast reactor. Even if the use of this high-order method becomes more frequent, for example within the APOLLO-3 code (Rimpault et al., 2014), collision probabilities are still used for many practical calculations and they define the scope of this article.

It seems that the attractiveness of those models has been growing recently driven by the heterogeneous design of some new nuclear reactors. For sodium fast breeder reactors, the presence of fertile assemblies or blankets may induce large shifts in the neutron spectrum together with an important streaming from the fissile to the fertile zones. The infinite lattice calculation of such a subcritical assembly (or of non-multiplicative ones) is often done within a "cluster" by surrounding it by a fissile material that acts as the neutron source. The question of a leakage model capable of handling those geometries correctly is to be asked. Moreover, given that sodium is more transparent to neutrons than water and that fast neutrons have a larger mean free path, it is easily seen that an adequate simulation of neutron streaming is required when modeling such reactors.

In the present work, the impact of the leakage model is discussed for the generation of homogenized and condensed cross sections and diffusion coefficients to be used in sodium fast reactor analysis. In Section 2, the neutron transport equation is presented and equations are derived for the B_1 homogeneous and the TIBERE models. The methodology for assembly calculation with the DRAGON-3 code is presented in Section 3 together with some comparisons with a reference Monte Carlo simulation. Group constants as a function of the leakage model are compared in Section 4 and Section 5 gives numerical results for simple sodium fast reactor cores calculations.

2. Neutron leakage in lattice theory and B_1 equations

Starting from the neutron transport equation presented in Section 2.1, the homogeneous B_1 leakage model and the heterogeneous TIBERE model are derived respectively in Sections 2.2 and 2.3.

2.1. The neutron transport equation

The multigroup neutron transport equation for the angular flux $\phi^g(\vec{r},\vec{\Omega})$ is often written in the form of an eigenvalue problem:

$$\left(\vec{\Omega}\cdot\vec{\nabla}+\Sigma^g(\vec{r})\right)\phi^g(\vec{r},\vec{\Omega})=q^g_{[\phi]}(\vec{r},\vec{\Omega}) \tag{1}$$

where $\Sigma^g(\vec{r})$ is the macroscopic total cross section and $q^g_{[\phi]}(\vec{r},\vec{\Omega})$ is the neutron source density that can be expressed in terms of the differential scattering and production cross sections $\Sigma_s^{g'\to g}(\vec{r},\vec{\Omega}'\to\vec{\Omega})$ and $\nu\Sigma_f^{g'}(\vec{r})$ as:

$$q^g_{[\phi]}(\vec{r},\vec{\Omega})=\sum_{g'}\int_{4\pi}d^2\Omega'\Sigma_s^{g'\to g}(\vec{r},\vec{\Omega}'\to\vec{\Omega})\phi^{g'}(\vec{r},\vec{\Omega}')+\frac{\chi^g(\vec{r})}{4\pi K}\sum_{g'}\nu\Sigma_f^{g'}(\vec{r})\phi^{g'}(\vec{r})$$

The angular flux $\phi^g(\vec{r},\vec{\Omega})$ and the multiplication factor K are the unknowns of the problem, namely the eigenfunction and the eigenvalue. We also use $\chi^g(\vec{r})$ the fission spectrum and $\phi^g(\vec{r})$ the scalar flux defined by:

$$\phi^g(\vec{r})=\int_{4\pi}d^2\Omega\phi^g(\vec{r},\vec{\Omega})$$

If neutron leakage is not taken into account, (1) is solved directly to compute the flux and the following definition is used for the diffusion coefficient:

$$D^g(\vec{r})=\frac{1}{3\left(\Sigma^g(\vec{r})-\Sigma^g_{s,1}(\vec{r})\right)} \tag{2}$$

where $\Sigma^g_{s,1}(\vec{r})$ is the first Legendre polynomial moment of the scattering cross section. Otherwise, a solution for (1) is sought in the form:

$$\phi^g(\vec{r},\vec{\Omega})=\varphi^g(\vec{r},\vec{\Omega})e^{i\vec{B}\cdot\vec{r}} \tag{3}$$

where $\varphi^g(\vec{r},\vec{\Omega})$ is a lattice-periodic complex-valued distribution called "microscopic flux" and $\vec{B}$ an invariant vector that represents the macroscopic curvature of the flux within the core. A new eigenvalue problem that involves a correction for neutron leakage is then generated:

$$\left(\vec{\Omega}\cdot\vec{\nabla}+\Sigma^g(\vec{r})+i\vec{\Omega}\cdot\vec{B}\right)\varphi^g(\vec{r},\vec{\Omega})=q^g_{[\varphi]}(\vec{r},\vec{\Omega}) \tag{4}$$

The angular dependence of the leakage probability $i\vec{\Omega}\cdot\vec{B}$ makes Eq. (4) incompatible with the traditional collision probability method. Further developments are therefore needed if such a method is to be used for lattice calculations.

2.2. The homogeneous B_1 leakage model

2.2.1. Modified neutron transport equation

The homogeneous leakage model overcomes the difficulty mentioned above by replacing the general leakage probability by that for a homogeneous media that appears to be isotropic. Within the B_1 leakage model, the scattering differential cross section is also developed to first order in Legendre polynomials and it is possible to show that for an infinite homogeneous media, and after the angular integration has been performed, Eq. (4) becomes:

$$\Sigma^g\varphi^g=\frac{\chi^g}{K}\sum_{g'}\nu\Sigma_f^{g'}\varphi^{g'}+\sum_{g'}\Sigma_{s,0}^{g'\to g}\varphi^{g'}-iBj^g \tag{5}$$

with B the modulus of $\vec{B}$, $\Sigma_{s,0}^{g'\to g}$ the zeroth moment of the differential scattering cross section, φ^g the homogeneous scalar flux and j^g the projection of the current in the direction of $\vec{B}$ given by:

$$j^g=\frac{\vec{j}^{\,g}\cdot\vec{B}}{B}=\frac{1}{B}\int_{4\pi}d^2\Omega\varphi^g(\vec{\Omega})\vec{\Omega}\cdot\vec{B}$$

If one follows the definition of Deniz (1986) for the diffusion coefficient D^g, which consists in equating the ratio leakage rate/flux to $D^g B^2$

$$\frac{iBj^g}{\varphi^g} = D^g B^2 \tag{6}$$

one obtains:

$$D^g = \frac{i}{B}\frac{j^g}{\varphi^g} \tag{7}$$

Using (6) in (4) one obtains the new (heterogeneous) transport equation:

$$\left(\vec{\Omega}\cdot\vec{\nabla} + \Sigma^g(\vec{r}) + D^g B^2\right)\varphi^g(\vec{r},\vec{\Omega}) = q^g_{[\varphi]}(\vec{r},\vec{\Omega}) \tag{8}$$

Assuming an isotropic source distribution (e.g. a zeroth order development for the scattering cross section), Eq. (8) can now be solved with the collision probability method. In the DRAGON-3 code, a non-leakage probability P^g_{NL} defined as a function of the homogenized total and within group scattering cross sections (zeroth order) is introduced:

$$P^g_{NL} = \frac{\Sigma^g - \Sigma^{g\to g}_{s,0}}{\Sigma^g - \Sigma^{g\to g}_{s,0} + D^g B^2}$$

The equations to be solved are then written:

$$V_j\varphi^g_j - \sum_i p^g_{ij} V_i \Sigma^{g\to g}_{s,0,i}\varphi^g_i = P^g_{NL}\sum_i p^g_{ij} V_i \hat{q}^g_{[\varphi],i} \tag{9}$$

where the indices i and j correspond to discretized regions of the geometry (volumes V_i and V_j) and p^g_{ij} is the classical reduced collision probability whose definition is provided in the appendix. The source density $\hat{q}^g_{[\varphi],i}$ excludes the contributions from within group scattering and is written:

$$\hat{q}^g_{[\varphi],i} = \sum_{g'\neq g}\Sigma^{g'\to g}_{s,0,i}\varphi^g_i + \frac{\chi^g_i}{K}\sum_{g'}\nu\Sigma^{g'}_{f,i}\varphi^{g'}_i$$

This equation uses transport corrected total and scattering cross sections.

2.2.2. Critical buckling search

Eq. (9) (or (8)) can be solved in such a way as to obtain a critical solution for the flux ($K = 1$). The diffusion coefficient D^g and buckling B^2 are calculated at the end of each outer iteration by searching for a solution $\{B, \phi^g, j^g\}$ of the coupled homogeneous B_1 system of equations (derivation given in Hébert (2009)):

$$\begin{cases} \Sigma^g\varphi^g = \frac{\chi^g}{K}\sum_{g'}\nu\Sigma^{g'}_f\varphi^{g'} + \sum_{g'}\Sigma^{g'\to g}_{s,0}\varphi^{g'} - iBj^g \\ i\Sigma^g\frac{j^g}{B} = \frac{1}{\gamma[B,\Sigma^g]}\left(i\sum_{g'}\Sigma^{g'\to g}_{s,1}\frac{j^{g'}}{B} + \frac{1}{3}\varphi^g\right) \end{cases} \tag{10}$$

where the cross sections and fission spectrum are homogenized from the heterogeneous motif using a classical flux/volume weighting and the term $\gamma[B,\Sigma^g]$ is given by:

$$\gamma[B,\Sigma^g] = \frac{B^2}{3\Sigma^g}\frac{\alpha[B,\Sigma^g]}{(1-\alpha[B,\Sigma^g]\Sigma^g)} \tag{11}$$

with:

$$\alpha[B,\Sigma^g] = \frac{1}{4\pi}\int_{4\pi} d^2\Omega \frac{\Sigma^g}{(\Sigma^g)^2 + (\vec{\Omega}\cdot\vec{B})^2}$$

Thus, by combining heterogeneous flux calculation and homogeneous buckling search, a critical distribution for the flux can be obtained.

2.3. The heterogeneous TIBERE model

The TIBERE model is a simplified B_1 leakage model compatible with the collision probability method and capable of taking into account local leakage by computing directional currents over the heterogeneous motif. The derivation of this model, given in Petrovic and Benoist (1997), is recalled here. It assumes that the cells or assemblies have three orthogonal planes of symmetry.

2.3.1. Modified transport equations

In the TIBERE model, a solution of (4) is sought under a first order power series expansion in terms of the buckling:

$$\varphi^g(\vec{r},\vec{\Omega}) = \varphi^g_s(\vec{r},\vec{\Omega}) - i\sum_{k=x,y,z} B_k\varphi^g_{ak}(\vec{r},\vec{\Omega}) \tag{12}$$

Introducing (12) in (4), separating the real from the imaginary part and assuming a first order development in Legendre polynomials for the scattering cross section, we obtain:

$$\begin{cases} \left(\vec{\Omega}\cdot\vec{\nabla} + \Sigma^g(\vec{r})\right)\varphi^g_s(\vec{r},\vec{\Omega}) = \frac{1}{4\pi}\sum_{g'}\hat{\Sigma}^{g'\to g}_0(\vec{r})\varphi^{g'}_s(\vec{r}) \\ \quad + \frac{3}{4\pi}\sum_{g'}\Sigma^{g'\to g}_{s,1}(\vec{r})\vec{j}^{\,g'}_s(\vec{r})\cdot\vec{\Omega} - \vec{B}\cdot\vec{\Omega}\sum_k B_k\varphi^g_{ak}(\vec{r},\vec{\Omega}) \\ \left(\vec{\Omega}\cdot\vec{\nabla} + \Sigma^g(\vec{r})\right)\varphi^g_{ak}(\vec{r},\vec{\Omega}) = \frac{1}{4\pi}\sum_{g'}\hat{\Sigma}^{g'\to g}_0(\vec{r})\varphi^{g'}_{ak}(\vec{r}) \\ \quad + \frac{3}{4\pi}\sum_{g'}\Sigma^{g'\to g}_{s,1}(\vec{r})\vec{j}^{\,g'}_{ak}(\vec{r})\cdot\vec{\Omega} + \varphi^g_s(\vec{r},\vec{\Omega})\Omega_k \end{cases} \tag{13}$$

where:

$$\begin{cases} \varphi^g_s(\vec{r}) = \int_{4\pi} d^2\Omega\varphi^g_s(\vec{r},\vec{\Omega}) \\ \varphi^g_{ak}(\vec{r}) = \int_{4\pi} d^2\Omega\varphi^g_{ak}(\vec{r},\vec{\Omega}) \\ \vec{j}^{\,g}_s(\vec{r}) = \int_{4\pi} d^2\Omega\varphi^g_s(\vec{r},\vec{\Omega})\vec{\Omega} \\ \vec{j}^{\,g}_{ak}(\vec{r}) = \int_{4\pi} d^2\Omega\varphi^g_{ak}(\vec{r},\vec{\Omega})\vec{\Omega} \end{cases}$$

and:

$$\hat{\Sigma}^{g'\to g}_0(\vec{r}) = \Sigma^{g'\to g}_{s,0}(\vec{r}) + \frac{\chi^g(\vec{r})}{K}\nu\Sigma^{g'}_f(\vec{r})$$

In order to solve this system, some hypothesis for the angular distribution of $\varphi^g_s(\vec{r},\vec{\Omega})$ and $\varphi^g_{ak}(\vec{r},\vec{\Omega})$ are required and some anti-symmetric terms are replaced by their averaged values at the scale of the cell or assembly (they are zero) in the right side of (13). A fitting correction is also introduced in order to match the homogeneous B_1 model for a homogeneous motif and the set of coupled B_1 equations for the TIBERE model is obtained:

$$\begin{cases} \left(\vec{\Omega}\cdot\vec{\nabla} + \Sigma^g(\vec{r})\right)\varphi^g_s(\vec{r},\vec{\Omega}) = \sum_{g'}\hat{\Sigma}^{g'\to g}_0\varphi^{g'}_s(\vec{r}) \\ \quad - \frac{3}{4\pi}\sum_k B_k^2 j^g_{akk}(\vec{r})\Omega_k^2 \\ \left(\vec{\Omega}.\vec{\nabla} + \Sigma^g(\vec{r})\right)\varphi^g_{ak}(\vec{r},\vec{\Omega}) = \frac{1}{\gamma[B,\Sigma^g]}\times \\ \quad \left(\frac{3}{4\pi}\sum_{g'}\hat{\Sigma}^{g'\to g}_1(\vec{r})j^{g'}_{akk}(\vec{r})\Omega_k + \frac{1}{4\pi}\varphi^g_s(\vec{r})\Omega_k\right) \end{cases} \tag{14}$$

where $j^g_{akk}(\vec{r})$ is the projection of $\vec{j}^{\,g}_{ak}$ over the axis k, $\gamma[B,\ \Sigma^g]$ is the factor introduced in (11) with Σ^g the homogenized total cross section and $\hat{\Sigma}^{g'\to g}_1(\vec{r})$ a modified first order scattering cross section given by:

$$\hat{\Sigma}^{g'\to g}_1(\vec{r}) = \Sigma^{g'\to g}_{s,1}(\vec{r}) + \delta_{g,g'}\left(1-\gamma[B,\Sigma^{g'}]\right)\left(\Sigma^{g'} - \Sigma^{g'}(\vec{r})\right)$$

The coupled system formed by the four equations in (14) can be put in a form compatible with the collision probability method.

The model implemented in the DRAGON-3 code assumes a "quasi-isotropic boundary condition" (Petrovic et al, 1996) and can be written:

$$\begin{cases} V_j\Sigma_j\varphi^g_{s,j} = \sum_i V_i\left(\widehat{P}^g_{ij}\sum_{g'}\hat{\Sigma}^{g'\to g}_{0,i}\varphi^g_{s,i} - \sum_k B^2_k P^{*g}_{ijk} j_{akk,i}\right) \\ V_j\Sigma_j j^g_{akk,j} = \frac{1}{\gamma[B,\Sigma^g_H]}\times\sum_i V_i\left(\sum_{g'}\hat{\Sigma}^{g'\to g}_{1,i} j^g_{akk,i} + \frac{1}{3}\varphi^g_{s,i}\right)\widehat{P}^g_{ijk} \end{cases} \quad (15)$$

where i and j are used to identify regions of the geometry and the collision probabilities $\widehat{P}^g_{ij}$, P^{*g}_{ijk} and $\widehat{P}^g_{ijk}$ are given in the appendix.

The local directional diffusion coefficients are then defined as:

$$D^g_k(\vec{r}) = \frac{j^g_{akk}(\vec{r})}{\varphi^g_s(\vec{r})} \quad (16)$$

2.3.2. Critical buckling search

In the TIBERE model, the flux and directional current distributions are directly computed over the heterogeneous motif. $K = 1$ is used at the beginning of the calculation and, assuming the three buckling components are equal, the neutron balance (first equation of (15)) is used to deduce a new value for B^2 at the end of each outer iteration.

3. Calculation of SFR assemblies with DRAGON-3

In this section, the modeling of four sodium cooled fast reactor assemblies is considered with the deterministic code DRAGON-3. A fissile, a fertile and two reflector assemblies are considered in Section 3.1. The main features of these assemblies are inspired from Blanchet et al. (2011) even though the geometries are not rigorously identical. Some elements of comparison with the results of a reference calculation performed with the SERPENT-1 stochastic code are given in Section 3.2 and the performance of DRAGON-3 is discussed in Section 3.3.

3.1. Description of geometry and physical modeling

For all assemblies, a 315 group ENDF/B-VII based nuclear cross section library is used with DRAGON. This library was derived by Alain Hébert for fast reactor applications. The self-shielding of resonant cross sections is taken into account using the generalized Stamm'ler method described in Hébert and Marleau (1991) and, in this section, the flux is calculated by the collision probability method without any leakage model. Homogenization and condensation are performed using the classical flux/volume weighting.

3.1.1. Fissile assembly

The fissile assembly is made up of a triangular lattice of 271 pins inserted in a hexagonal wrapper tube with sodium coolant. The geometrical features of the assembly and the isotopic composition of the different structures are summarized in Tables 1–3. The sodium density is $2.1924 \cdot 10^{-2}$ atoms/barn/cm and the respective temperatures of fuel and structure/coolant materials are 1500 K and 600 K.

For practical reasons, the external sodium blade is diluted within the wrapper tube material in the DRAGON-3 modeling (see Fig. 1). For the self-shielding calculation, only the heavy nuclides of the fuel are treated and it has been observed that a single resonant zone embracing all the pins gives satisfactory results.

3.1.2. Fertile assembly

The fertile assembly main characteristics are identical to those of the fissile assembly, with the exception that the fuel pellets are replaced by natural uranium oxide whose isotopic composition is given in Table 4. The fertile material temperature is 600 K.

Being subcritical, the motif is inserted in the hexagonal cluster composed of a central fertile zone and six fissile assemblies and depicted in Fig. 1. The surrounding assemblies are replaced by a homogeneous mixture whose properties are extracted from the homogenization of a fissile assembly. It was observed that resonance self-shielding of the fertile material can be performed using an isolated fertile assembly with one resonant zone without compromising the accuracy of the results.

3.1.3. Reflectors

Two types of reflectors are considered. The axial reflector is modeled in the same way as the fertile assembly but fuel pellets are replaced by EM10 steel (see Table 2). For the radial reflector, the assembly is assumed to be a homogeneous media whose composition is a mixture of EM10 steel and sodium with respective volumes ratio of 74% and 26%. In both cases, the flux calculation is performed over a cluster geometry (see Fig. 1).

Table 1
Geometry parameters for fuel assembly.

Geometry parameter	Value
Assembly pitch (cm)	21.2205
Duct outer flat-to-flat distance (cm)	20.7468
Duct thickness (cm)	0.4525
Number of pins	271
Fuel pin radius (cm)	0.4893
Outer clad radius (cm)	0.5419
Pin to pin distance (cm)	1.1897

Table 2
Isotopic composition of assembly structures.

Cladding (ODS steel)		Wrapper (EM10 steel)	
Nuclide	Density (at./barn/cm)	Nuclide	Density (at./barn/cm)
C^{12}	$3.5740 \cdot 10^{-4}$	C^{12}	$3.8254 \cdot 10^{-4}$
O^{16}	$3.9924 \cdot 10^{-4}$	Si	$4.9089 \cdot 10^{-4}$
Ti	$5.3824 \cdot 10^{-4}$	Ti	$1.9203 \cdot 10^{-5}$
Cr	$1.7753 \cdot 10^{-2}$	Cr	$7.5122 \cdot 10^{-3}$
Fe	$5.3872 \cdot 10^{-2}$	Fe	$7.3230 \cdot 10^{-2}$
Ni	$3.6588 \cdot 10^{-4}$	Ni	$3.9162 \cdot 10^{-4}$
Mn	$2.3441 \cdot 10^{-4}$	Mn	$4.1817 \cdot 10^{-4}$
P^{31}	$2.7718 \cdot 10^{-5}$	Mo	$4.7925 \cdot 10^{-4}$
Al^{27}	$9.1482 \cdot 10^{-3}$		
Co^{59}	$2.1852 \cdot 10^{-4}$		
Cu	$1.0135 \cdot 10^{-4}$		
Y	$2.6616 \cdot 10^{-4}$		

Table 3
Isotopic concentration of fissile fuel pellet.

Nuclide	Density (at./barn/cm)	Nuclide	Density (at./barn/cm)
O^{16}	$4.2825 \cdot 10^{-2}$	Pu^{242}	$3.1762 \cdot 10^{-4}$
U^{234}	$1.6555 \cdot 10^{-6}$	Am^{241}	$3.6419 \cdot 10^{-5}$
U^{235}	$2.9137 \cdot 10^{-5}$	Am^{242}	$1.5317 \cdot 10^{-8}$
U^{236}	$4.7679 \cdot 10^{-6}$	Am^{242*}	$1.3853 \cdot 10^{-6}$
U^{238}	$1.8322 \cdot 10^{-2}$	Am^{243}	$2.9501 \cdot 10^{-5}$
Np^{237}	$5.5220 \cdot 10^{-6}$	Cm^{242}	$2.7086 \cdot 10^{-6}$
Np^{239}	$4.8411 \cdot 10^{-6}$	Cm^{243}	$1.4828 \cdot 10^{-7}$
Pu^{238}	$8.6992 \cdot 10^{-5}$	Cm^{244}	$5.1600 \cdot 10^{-6}$
Pu^{239}	$1.8845 \cdot 10^{-3}$	Cm^{245}	$2.9876 \cdot 10^{-7}$
Pu^{240}	$1.0108 \cdot 10^{-3}$	Cm^{246}	$9.5184 \cdot 10^{-9}$
Pu^{241}	$2.0474 \cdot 10^{-4}$	Mo	$2.7413 \cdot 10^{-3}$

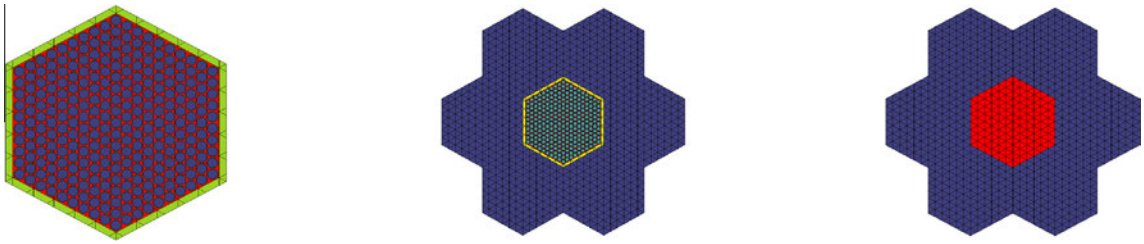

Fig. 1. Fissile assembly (left) and cluster model for a fertile and axial reflector (center) and for a radial reflector (right) assemblies.

Table 4
Isotopic concentration of fertile fuel pellet.

Nuclide	Density (at./barn/cm)
O^{16}	$4.72816 \cdot 10^{-2}$
U^{235}	$1.70214 \cdot 10^{-4}$
U^{238}	$2.34706 \cdot 10^{-2}$

Table 5
K_∞ for fissile assembly.

	SERPENT	DRAGON
K_∞	1.15714 ± 3 pcm	1.16315
$\Delta\rho$ (pcm)		+ 447

3.2. Comparison with reference Monte Carlo calculations

The fissile assembly of Section 3.1.1 is calculated with DRAGON-3 and the results compared to a reference solution of the problem obtained with the SERPENT-1 code (Monte Carlo method). The infinite lattice multiplication factor K_∞ and the 315 group homogenized flux spectrum are respectively given in Table 5 and in Fig. 2. The reactivity error (in pcm) is also computed as:

$$\Delta\rho = 10^5\left(\frac{1}{K_\infty^{\text{SERPENT}}} - \frac{1}{K_\infty^{\text{DRAGON}}}\right)$$

For the Monte Carlo calculation, the results are presented together with standard deviations (1σ for K_∞ and 3σ for the flux and cross sections).

We see that DRAGON-3 overestimates the reactivity by about 450 pcm. A good agreement is observed for the flux energy spectrum. It is also observed that the number of neutrons slowing down under 100 eV is very small. From this fact, a 24 group energy structure, inspired from the 33 group ECCO structure, is adopted for further cross-section condensation (see Table 6). In this condensed structure, we see that the DRAGON-3 flux spectrum, illustrated in Fig. 3, is slightly harder than the SERPENT-1 one. Except for some specific groups (e.g. 7, 10 and 11), the DRAGON-3 spectrum globally agrees with the reference result.

In Figs. 4–6 the total, absorption and production cross sections homogenized over the assembly and condensed to the 24 group energy structure are presented. The relative differences (in %) between the DRAGON and SERPENT results given by:

$$\Delta_r = 100\frac{X^{\text{DRAGON}} - X^{\text{SERPENT}}}{X^{\text{SERPENT}}}$$

are also provided in these figures.

In most groups, the total cross section calculated with DRAGON agrees with the SERPENT results within 1%. Larger relative differences are found in groups 9, 10, 11 and 17 (1.4–2.7%) and in group 24 (4.9%) where the neutron density is very small. For the absorption cross section we see that the relative differences between the

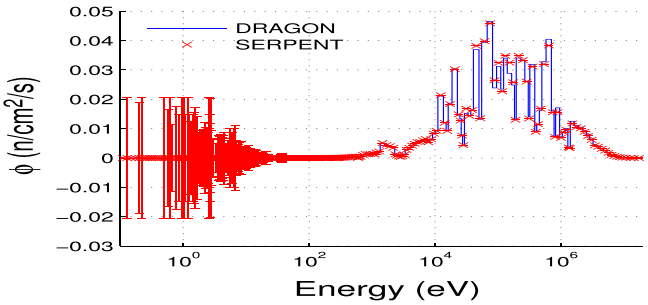

Fig. 2. 315 group flux spectrum for fissile assembly.

Table 6
24 group energy structure for condensation.

G	Upper limit (eV)	Lower limit (eV)
1	$20.00000 \cdot 10^6$	$10.00000 \cdot 10^6$
2	$10.00000 \cdot 10^6$	$6.065307 \cdot 10^6$
3	$6.065307 \cdot 10^6$	$3.678794 \cdot 10^6$
4	$3.678794 \cdot 10^6$	$2.231302 \cdot 10^6$
5	$2.231302 \cdot 10^6$	$1.353353 \cdot 10^6$
6	$1.353353 \cdot 10^6$	$8.208500 \cdot 10^5$
7	$8.208500 \cdot 10^5$	$4.978707 \cdot 10^5$
8	$4.978707 \cdot 10^5$	$3.019738 \cdot 10^5$
9	$3.019738 \cdot 10^5$	$1.831564 \cdot 10^5$
10	$1.831564 \cdot 10^5$	$1.110900 \cdot 10^5$
11	$1.110900 \cdot 10^5$	$6.737947 \cdot 10^4$
12	$6.737947 \cdot 10^4$	$4.086771 \cdot 10^4$
13	$4.086771 \cdot 10^4$	$2.478752 \cdot 10^4$
14	$2.478752 \cdot 10^4$	$1.503439 \cdot 10^4$
15	$1.503439 \cdot 10^4$	$9.118820 \cdot 10^3$
16	$9.118820 \cdot 10^3$	$5.530844 \cdot 10^3$
17	$5.530844 \cdot 10^3$	$3.354626 \cdot 10^3$
18	$3.354626 \cdot 10^3$	$2.034684 \cdot 10^3$
19	$2.034684 \cdot 10^3$	$1.234098 \cdot 10^3$
20	$1.234098 \cdot 10^3$	$7.485183 \cdot 10^2$
21	$7.485183 \cdot 10^2$	$4.539993 \cdot 10^2$
22	$4.539993 \cdot 10^2$	$3.043248 \cdot 10^2$
23	$3.043248 \cdot 10^2$	$1.486254 \cdot 10^2$
24	$1.486254 \cdot 10^2$	$1.000000 \cdot 10^{-5}$

deterministic and the reference calculation are somewhat larger: 3.8% and −3.4% in groups 1 and 17, 10.4% in group 20 and up to 7.7% for the most thermal group. In all other groups, the relative differences remain less than 1%. For the production cross section ($\nu\Sigma_f$) a good agreement between both codes is found with relative differences smaller than 1% in all groups except groups 20, 21 and 24 (respectively 3.6%, −2.0% and 3.1%).

3.3. Discussion

The methodology presented in this section is able to generate homogenized and condensed cross section for a fast reactor

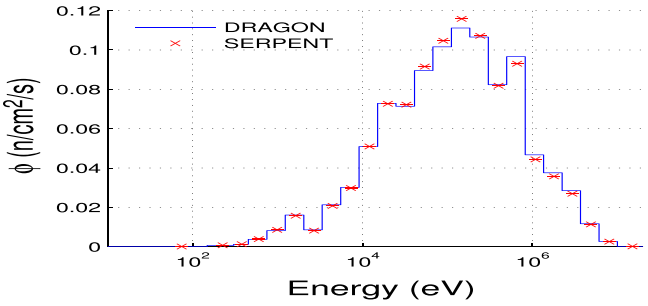

Fig. 3. 24 group flux spectrum for fissile assembly.

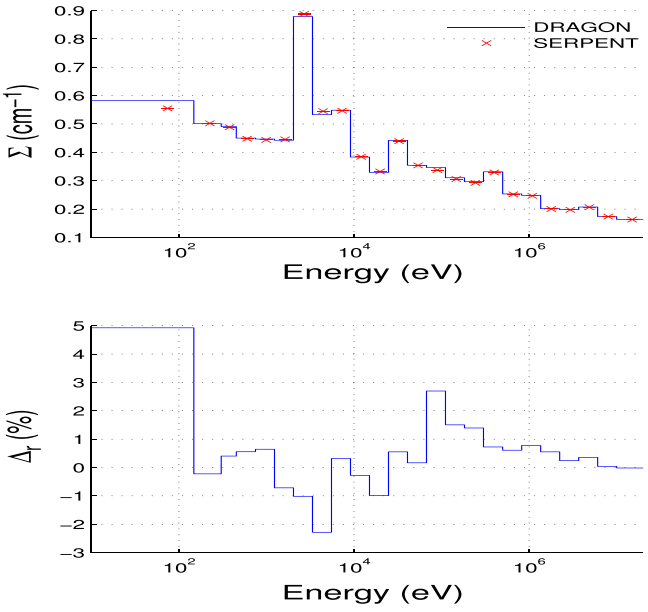

Fig. 4. Homogenized total cross section for fissile assembly. Cross section values (top) and relative differences between DRAGON and SERPENT (bottom).

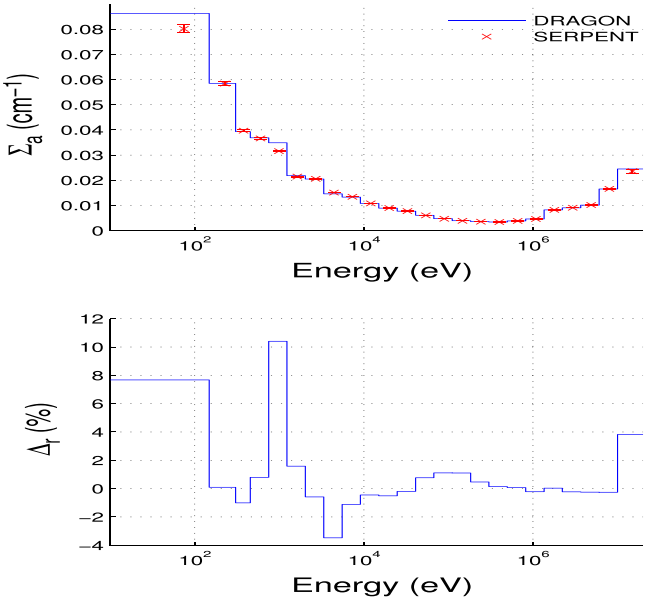

Fig. 5. Homogenized absorption cross section for fissile assembly. Cross section values (top) and relative differences between DRAGON and SERPENT (bottom).

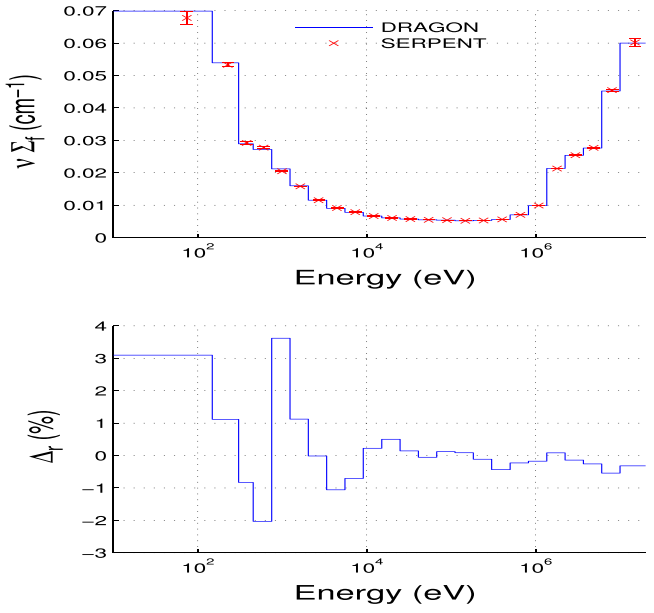

Fig. 6. Homogenized production cross section for fissile assembly. Cross section values (top) and relative differences between DRAGON and SERPENT (bottom).

assembly that are generally in agreement with the results obtained using a Monte Carlo simulations (1% error bar). Some improvement could be achieved by using a more refined energy structure for the DRAGON library (e.g. 1968 groups). The use of a subgroup method for resonance self-shielding calculations, recommended in Rimpault et al. (2014), could also help decrease the relative differences observed in some groups. However, the purpose of the current work is not to present the most precise calculation scheme for fast reactors. The accuracy of our DRAGON-3 model is considered adequate for evaluating the performance of the different leakage models presented in Section 2.

4. Group constant generation: impact of the leakage model

Here, the general impact of the leakage model selected for the critical flux calculation is analyzed. Global effects on the infinite lattice multiplication factor and on the homogenized flux spectrum are first illustrated in Section 4.1 for the fissile assembly. In Section 4.2 homogenized and condensed cross sections are discussed. Diffusion coefficients are reported in Section 4.3 for the fissile assembly and the cluster calculation of a fertile assembly. The results are discussed in Section 4.4.

4.1. Flux spectrum and multiplication factor

Three flux calculations are performed for the fissile assembly of Section 3.1.1: without neutron leakage, with the B_1 homogeneous model and with the B_1 heterogeneous TIBERE model. For these last two cases, a critical buckling search is performed. Table 7 presents the values of the infinite multiplication factor K_∞ and of the buckling B^2. Fig. 7 shows the homogenized flux spectrum, condensed to the 24 group energy structure, as well as the relative difference (in %) between the infinite lattice with and without leakage:

$$\Delta_r = 100\frac{X^{B_1} - X^{\text{No Leak}}}{X^{\text{No Leak}}}$$

We see that taking into account neutron leakage hardens the spectrum: the neutron flux is about 10% higher above 1 MeV and about 20% lower under 100 eV. However, the homogeneous and

Table 7
K_∞ and buckling for fissile assembly.

	No Leak	B_1 Hom	B_1 Het
K_∞	1.16315	1.22110	1.22165
$\Delta\rho$ (pcm)		+ 4080	+ 4116
B^2 (cm^{-2})	0.0	$1.17 \cdot 10^{-3}$	$1.16 \cdot 10^{-3}$

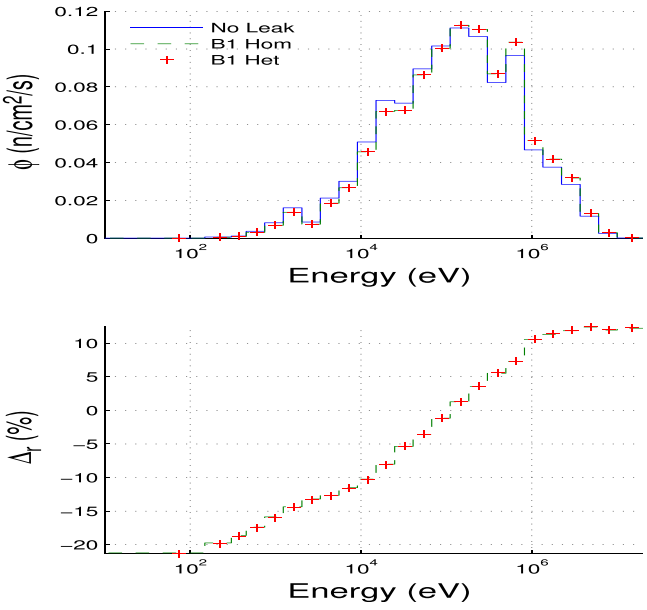

Fig. 7. Effect of leakage models on flux spectrum for fissile assembly. Flux values (top) and relative differences between specific leakage model and no leakage model (bottom).

heterogeneous leakage models are hardly different. As for the eigenvalue, the use of a leakage model results in an increase in reactivity of about 4100 pcm. No significant differences are observed between the two leakage models for the reactivity and buckling.

4.2. Homogenized and condensed cross section

Figs. 8 and 9 illustrate the homogenized 24 group total and production cross sections for different leakage models as well as the relative changes in these cross sections with respect to the case with no leakage.

The overlap of the different plots shows that the leakage model has a very low impact on homogenized cross sections. For the total cross section, the maximal relative difference Δ_r is less than 0.1%. For the production cross section, it is inferior to 0.2%. These differences are not significant given those observed in Section 3 between DRAGON and SERPENT calculations.

Similar results were observed for the other cross sections and for the other types of assemblies (not presented here). For the fertile and reflector assemblies, cross sections were obtained using a partial homogenization over the corresponding region of the cluster.

4.3. Diffusion coefficients

Depending on the leakage model, the diffusion coefficients are computed using Eq. (2), (7) or (16). For the heterogeneous leakage model, the radial D_r and axial D_z coefficients are evaluated independently. Figs. 10 and 11 show respectively the 24 group diffusion coefficients for a fissile and a fertile assembly.

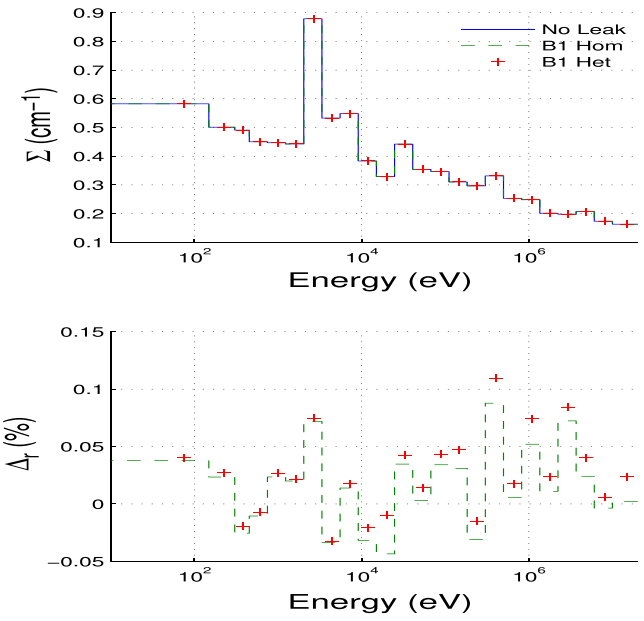

Fig. 8. Effect of leakage model on total cross section for fissile assembly. Cross section values (top) and relative differences between specific leakage models and no leakage model (bottom).

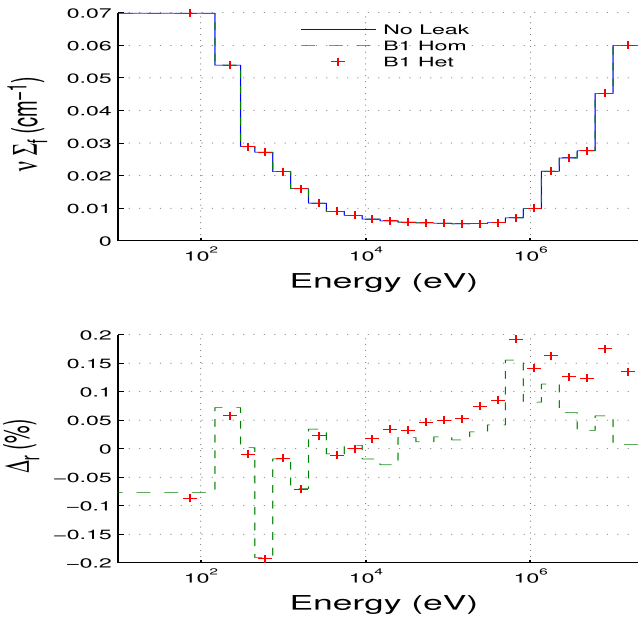

Fig. 9. Effect of leakage models on production cross section for fissile assembly. Cross section values (top) and relative differences between specific leakage models and no leakage model (bottom).

The impact of the leakage model on the diffusion coefficients is much more important than for the cross sections. For the fissile assembly, the differences generally remain between 1% and 5%. It can reach 25% in group 18 because of the resonant scattering behavior of ^{23}Na around 2.85 keV: the increase in the total cross section (see Fig. 8) implies a decrease in the diffusion coefficient when defined with Eq. (2). In most groups, the diffusion coefficients computed using the heterogeneous TIBERE model are the largest and they present a slight anisotropy ($D_z > D_r$).

For the fertile assembly, the impact of the leakage model is even more important. Above 500 keV, the heterogeneous leakage coefficients increase more rapidly with energy than the other ones: in

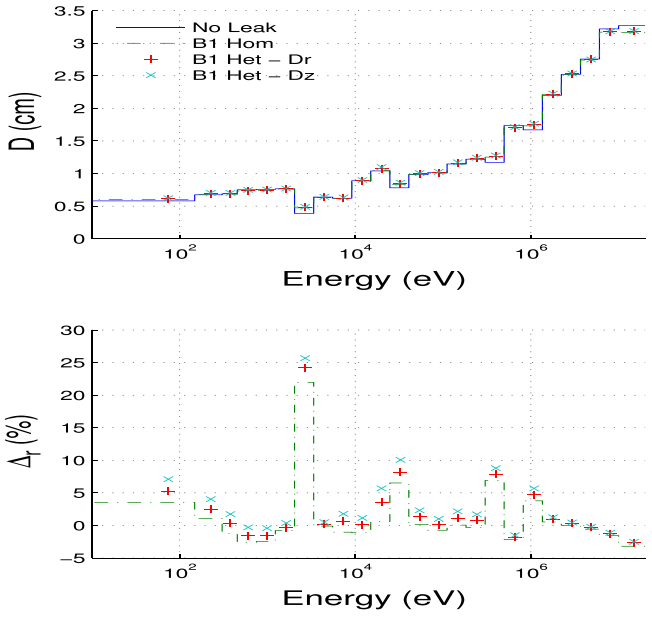

Fig. 10. Diffusion coefficients for fissile assembly. Coefficient values (top) and relative differences between specific leakage models and no leakage model (bottom).

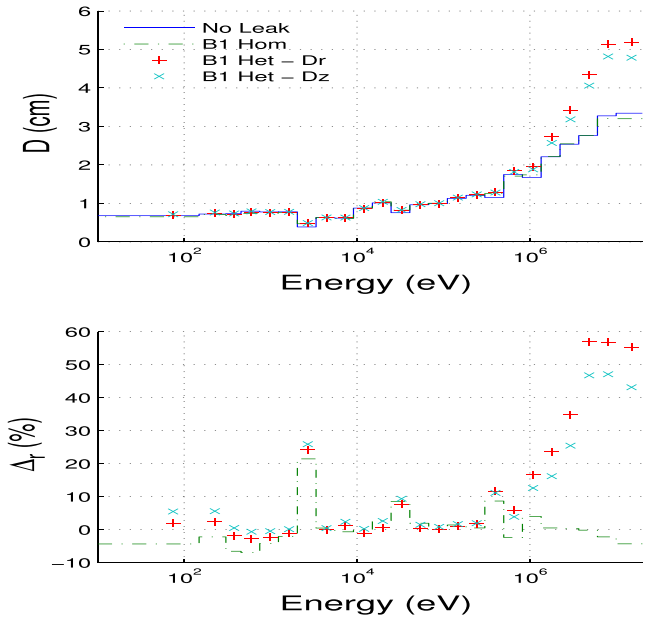

Fig. 11. Diffusion coefficients for fertile assembly. Coefficient values (top) and relative differences between specific leakage models and no leakage model (bottom).

the fastest groups, they are about 50% larger. For this case, radial streaming prevails ($D_r > D_z$).

Similar results are found for the reflector assemblies (Faure, 2016).

4.4. Discussion

The introduction of neutron leakage in the infinite lattice causes a shift in the flux spectrum that becomes harder. This shift has no significant impact on the 24 group condensed and homogenized cross sections because it does not change significantly the local structure of the multigroup flux within a macro-group.

However, the leakage model has a significant impact on the diffusion coefficients since the definition of these quantities is highly dependent on the model selected. Furthermore, for a cluster calculation, the validity of the homogeneous diffusion coefficient is highly questionable since its definition arises from homogenization over the entire cluster including the fissile assemblies. Besides, the cluster geometry suggests that there are neutrons streaming toward the fertile zone from the surrounding fissile assemblies, a phenomenon that cannot be taken into account without a heterogeneous leakage model. This explains the large increase in the directional leakage coefficients for the fast groups observed in Fig. 11. As for the homogeneous diffusion coefficient, its behavior is similar to the one computed with (2).

5. Calculation of SFR cores

In this section, two SFR cores are simulated using the diffusion code DONJON-5. Cross sections and diffusion coefficients are calculated for the reference assemblies without taking leakage into account and with the homogeneous or heterogeneous leakage models. The results are compared with a continuous energy Monte Carlo simulation performed over the heterogeneous geometry of each core. Section 5.1 presents the results for a homogeneous core. In Section 5.2, a simple heterogeneous core with reflectors and a fertile zone is presented. The results are discussed in Section 5.3.

5.1. Homogeneous core

The core under consideration is made up of 61 fissile assemblies (see Section 3.1.1) distributed in five crowns. Its height is $H = 311.16$ cm. The resulting effective multiplication factor K_{eff} as a function of the leakage model used for group constant generation is compared with the reference solution obtained with SERPENT-1 in Table 8. Fig. 12 shows the flux spectrum in an inner

Table 8
K_{eff} for homogeneous core.

	K_{eff}	$\Delta\rho$ (pcm)
SERPENT	1.03355 ± 3 pcm	/
No Leak	1.03903	+ 510
B_1 Hom	1.04245	+ 826
B_1 Het	1.04170	+ 757

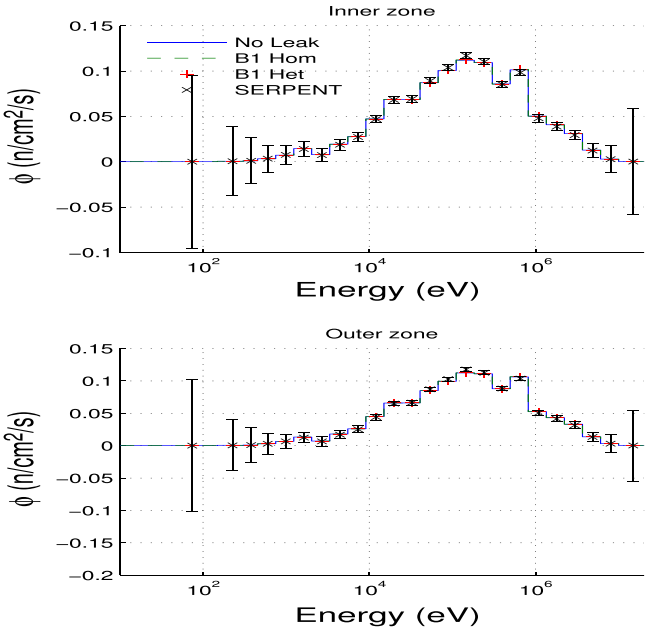

Fig. 12. 24 group flux spectrum in homogeneous core.

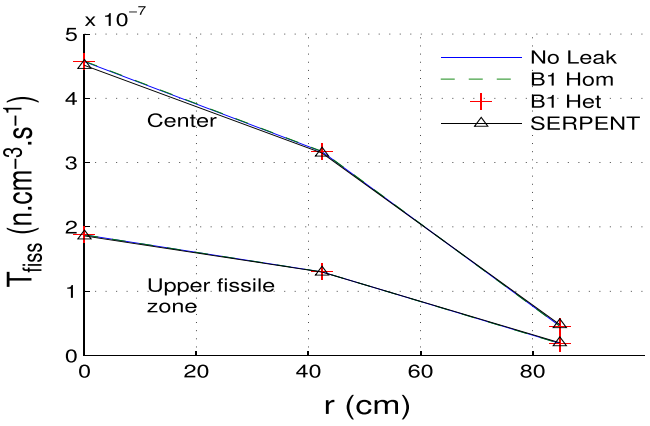

Fig. 13. Fission rate as a function of radial position for homogeneous core.

and an outer zone of the core. In Fig. 13, the radial fission rate distribution is given in the mid-plane and in the upper fissile zone of the core.

The best result for the eigenvalue is given for the calculation scheme that does not involve a leakage model ($\Delta\rho = +510$ pcm). The homogeneous leakage model introduces an additional reactivity difference of 316 pcm that can be reduced by about 70 pcm if the TIBERE model is considered.

As for the flux energy and spatial distributions, there are no significant differences between the models used. The global shape of the spectrum is respected by the DONJON-5 calculation and we observe a good agreement for the fission rate distribution.

5.2. Simple heterogeneous core

The heterogeneous core we considered is made up of eight hexagonal crowns. The last two crowns contain reflector assemblies. The seven inner regions are fertile assemblies while the intermediate region is filled with fissile assemblies. The height of the active core is now 140.79 cm, which is about 50% smaller than the height of the homogeneous core. The heights of the upper and lower axial reflectors are respectively 80.45 cm and 89.92 cm. A top view of the core is provided in Fig. 14 (fissile assemblies in yellow, fertile zone in pink and reflectors in green). The eigenvalue as a function of the combination of leakage models used for fissile, fertile and reflector assembly simulations are presented in Table 9.

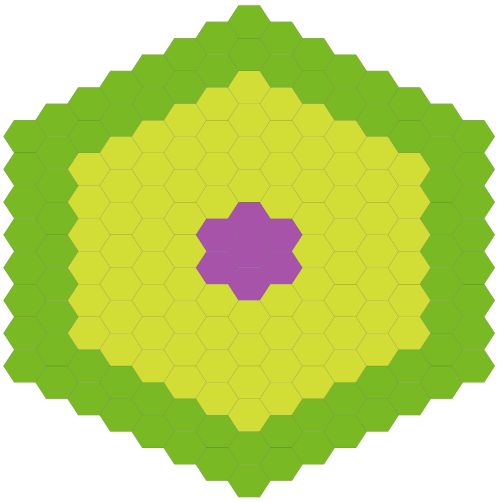

Fig. 14. Heterogeneous core viewed from the top.

The reference value calculated with SERPENT-1 is also given. Fig. 15 shows the neutron spectrum in a fissile and a fertile assembly located in the inner part of the core. The fission rate spatial distribution is depicted in Fig. 16 for three combinations of leakage models. In the first, no leakage model is used. In the second a homogeneous B_1 model is used only for reflector assemblies and in the last, clusters are calculated with the heterogeneous TIBERE model.

The best results for the eigenvalue are found when clusters (fertile and reflector assemblies) are calculated with the heterogeneous TIBERE model and no leakage model is used for the fissile assembly. For reflectors, the TIBERE model provides an improvement of 140 pcm in K_{eff} with respect to the case without leakage. The homogeneous model gives the worst results, the error being doubled. The difference in K_{eff} can be reduced by another 60–70 pcm by using a heterogeneous leakage model for the fertile assembly simulation.

Fig. 15 shows that the neutron spectrum is weakly dependent on the leakage model. In the fertile zone, the 3σ error bars of the SERPENT calculation are too large for the results to be trusted with great confidence despite the fact that the calculation lasted almost one month. This is due to the fact that neutrons are absorbed before reaching the central part of the core. In the fissile zone, we see that the spectrum is calculated with good accuracy even though an appreciable deviation can be observed in some energy groups. When it comes to the spatial distribution of the fission rate, the comparison of the plot corresponding to the absence of leakage models and the plot obtained with a heterogeneous model for cluster calculations show no significant difference. We also see that the use of a homogeneous model for calculating the reflector leads to an underestimation of the fission rates in the inner fissile zone of the core, where they reach their highest values.

5.3. Discussion

The results presented in this section show that it is possible to calculate a sodium fast reactor core with the diffusion code DONJON with an acceptable accuracy. However, the leakage model to be used for the infinite lattice calculation with DRAGON should be selected carefully in order to define consistent diffusion coefficients.

For cluster calculations (fertile or reflector assembly), it appears that the homogeneous B_1 leakage model leads to results that have relatively large errors in the eigenvalue and, to a lesser extent, in the fission rate distribution. This is due to the fact that the diffusion coefficient that arises from this leakage model is not consistent since its definition relies on homogenization over the entire cluster geometry. By comparing the results obtained without leakage model or with the TIBERE model, it was shown that the latter gives a better estimation of the eigenvalue. This comes from the fact that the directional leakage coefficients are computed as a function of the current (see Eq. (16)) and therefore adequately simulate neutron streaming between the different assemblies. The neutron spectrum is almost independent of the leakage model, from which we may infer that the improvement in eigenvalues comes from a better calculation of the leakage rate.

For fissile assembly calculations, we showed that the TIBERE model gives better results than the homogeneous leakage model. However, it appears the most accurate simulation is the one without leakage model. This fact was also observed by other authors (see Smith, 2016 where a critic is made of the B_1 leakage models).

Some questions can be raised about our use of a full-core Serpent reference solution. A first observation is that Monte Carlo simulations are generally considered to be more accurate than deterministic transport solutions because of the few approximations they imply (continuous energy, no need for spatial discretiza-

Table 9
K_{eff} for heterogeneous core.

SERPENT		$K_{eff} = 0.99626 \pm 2$ pcm		
DRAGON / DONJON				
FUEL	FERT	REFL	K_{eff}	$\Delta\rho$ (pcm)
No Leak		No Leak	1.00235	+ 610
		B_1 Hom	1.00679	+ 1050
		B_1 Het	1.00097	+ 472
No Leak	B_1 Hom	B_1 Het	1.00109	+ 484
	B_1Het		1.00035	+ 410
B_1 Hom	B_1 Het		1.00296	+ 671
B_1 Het			1.00255	+ 629

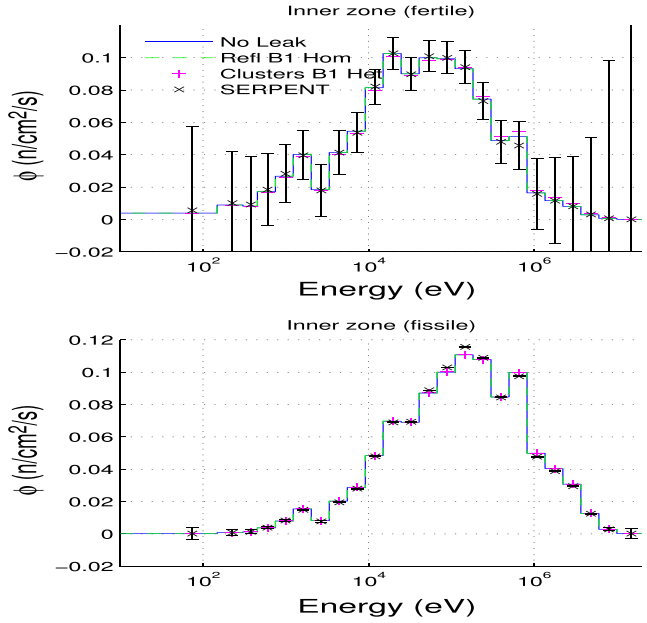

Fig. 15. 24 group flux spectrum in heterogeneous core.

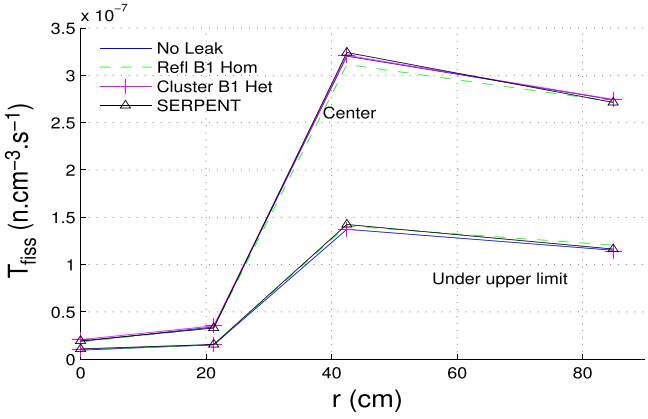

Fig. 16. Fission rate as a function of radial position for heterogeneous core.

tion or resonance self-shielding). As our goal is to evaluate how leakage models in transport affect the quality of the DONJON diffusion solution, using SERPENT to generate this reference solution was considered appropriate.

Another alternative for evaluating the reference full-core transport solution would be to use the code selected for the assembly and cluster calculations (i.e. DRAGON). The advantage of this strategy would be to circumvent the inherent differences observed in Section 3.2 between DRAGON and SERPENT. However, obtaining a converged 3D DRAGON solution implies a very fine mesh spatial discretization of the problem leading to a transport system involving several millions of unknowns. Limitations in computer resources and extremely long calculation time led us to the conclusion that obtaining such a solution was impractical.

Nevertheless, assuming that the reactivity difference of about 450 pcm presented in Table 5 provides a good estimate of the inherent difference between DRAGON and SERPENT we can further refine our analysis. By subtracting this reactivity offset due to DRAGON from the DONJON results presented in Table 8 for the homogeneous core, we see that the reactivity differences between SERPENT and DONJON decrease substantially. However, our previous conclusions regarding leakage models remain valid. Performing the same operation for the results of Table 9 indicates that the TIBERE model is still the best suited for calculating diffusion coefficients for the reflectors. For fertile assemblies, conclusions are harder to draw since the corrected reactivity differences between DONJON and SERPENT are small in all cases. This is not surprising since the volume of the fertile zone is relatively small compared to the other zones and even large changes in the diffusion coefficients associated with this region will only slightly impact the core eigenvalue.

6. Conclusion

In the present work, the traditional B_1 homogeneous model and the heterogeneous TIBERE model are compared for the generation of cross sections and diffusion coefficients to be used in sodium fast reactor analysis. Fissile, fertile and reflector assemblies are calculated with the lattice code DRAGON-3 using a 315 group energy structure. The homogenized parameters are condensed into 24 groups and a diffusion calculation is performed with the DONJON-5 code. Reference results are computed from independent Monte Carlo simulations.

It has been shown that leakage models have a low impact on cross sections but can significantly affect the diffusion coefficients. In particular, the homogeneous B_1 model should be avoided for cluster calculations since the resulting diffusion coefficients are not consistent with a partial homogenization. On the other hand, the TIBERE model is capable of calculating heterogeneous and anisotropic leakage coefficients that are best suited for simulating neutron streaming within such a geometry.

Furthermore, it has also been observed that leakage models give less accurate results than zero-buckling calculations for the generation of fissile assembly cross sections and diffusion coefficients. Further investigations should be made to understand the reason of this behavior even if some answers may be found in Smith (2016).

Finally, an article is in preparation that investigates the effect of leakage models for light water reactors (Faure, 2016). This work was performed in collaboration with the Commissariat à l'Energie Atomique et aux Energies Alternatives (Cadarache).

Acknowledgments

The authors acknowledge the Natural Sciences and Engineering Research Council of Canada (NSERC) for partly funding this work. One of the authors (B.F.) would like to thank the Commissariat à l'Energie Atomique et aux Energies Alternatives (CEA) for giving him the opportunity to work in Cadarache laboratory.

Appendix A. Appendix

The classical reduced collision probabilities for a neutron born in any of the regions i of the infinite lattice to undergo its first collision in region j can be written:

$$p_{ij} = \frac{1}{4\pi V_i} \int_{V_i^\infty} d^3r' \int_{V_j} d^3r \frac{e^{-\tau(s)}}{s^2}$$

where $s = |\vec{r}' - \vec{r}|$ and $\tau(s)$ is the optical path of the medium. The energy group indices g have been dropped here for the sake of simplicity.

In the TIBERE model with quasi-isotropic boundary conditions, the collision probabilities are calculated for an isolated cell:

$$P_{ij} = \frac{\Sigma_j}{4\pi V_i} \int_{V_i} d^3r' \int_{V_j} d^3r \frac{e^{-\tau(s)}}{s^2}$$

where the first integral is carried out over the volume i of one cell. The escape P_{iS}, penetration P_{Sj} and transmission P_{SS} probabilities through the cell surface S are also calculated as follows:

$$P_{iS} = \frac{1}{4\pi V_i} \int_{V_i} d^3r' \int_S d^2r_f (\vec{\Omega} \cdot \vec{N}_+) \frac{e^{-\tau(s)}}{s^2}$$

$$P_{Sj} = \frac{\Sigma_j}{\pi \xi_k S} \int_S d^2r_f \int_{V_j} d^3r (\vec{\Omega} \cdot \vec{N}_-) \frac{e^{-\tau(s)}}{s^2}$$

$$P_{SS} = \frac{1}{\pi \xi_k S} \int_S d^2r'_f \int_S d^2r_f (\vec{\Omega} \cdot \vec{N}_+)(\vec{\Omega} \cdot \vec{N}_-) \frac{e^{-\tau(s)}}{s^2}$$

with $\vec{N}_+$ and $\vec{N}_-$ the unit outgoing and incoming normal vectors on surface S and ξ_k a shape parameter written as:

$$\xi_k = \frac{3}{\pi S} \int_S d^2r_f \int_{2\pi} d^2\Omega |\Omega \cdot \vec{N}_+| \Omega_k^2$$

The directional collision probabilities are then given by:

$$P_{ijk} = \frac{3\Sigma_j}{4\pi V_i} \int_{V_i} d^3r' \int_{V_j} d^3r \frac{e^{-\tau(s)}}{s^2} \Omega_k^2$$

$$P_{iSk} = \frac{3}{4\pi V_i} \int_{V_i} d^3r' \int_S d^2r_f (\vec{\Omega} \cdot \vec{N}_+) \frac{e^{-\tau(s)}}{s^2} \Omega_k^2$$

$$P_{Sjk} = \frac{3\Sigma_j}{\pi \xi_k S} \int_S d^2r_f \int_{V_j} d^3r (\vec{\Omega} \cdot \vec{N}_-) \frac{e^{-\tau(s)}}{s^2} \Omega_k^2$$

$$P_{SSk} = \frac{3}{\pi \xi_k S} \int_S d^2r'_f \int_S d^2r_f (\vec{\Omega} \cdot \vec{N}_+)(\vec{\Omega} \cdot \vec{N}_-) \frac{e^{-\tau(s)}}{s^2} \Omega_k^2$$

and used to define the probabilities appearing in (15):

$$\widehat{P}_{ij} = P_{ij} + P_{iS} P$$

$$P^*_{ijk} = P_{ijk} + P_{iSk} P$$

$$\widehat{P}_{ijk} = P_{ijk} + P_{iSk} (1 - P_{SSk})^{-1} P_{Sjk}$$

$$P = (1 - P_{SS})^{-1} P_{Sj}$$

References

Behrens, D.J., 1949. The effect of holes in a reacting material on the passage of neutrons. Proc. Phys. Soc. London, Sect. A 62 (10), 607–616.

Benoist, P., 1961. Formulation générale et calcul pratique du coefficient de diffusion dans un réseau comportant des cavités. J. Nuclear Energy Part A 13 (34), 97–111.

Benoist, P., 1984. A simple model for the calculation of the sodium-voiding effect on neutron leakages in a fast reactor lattice. I. Formalism. Nuclear Sci. Eng. 86 (1), 22–40.

Benoist, P., 1986. Homogenization theory in reactor lattices. Tech. rep., CEA Centre d'Etudes Nucléaires de Saclay, 91-Gif-sur-Yvette (France). Inst. de Recherche Technologique et de Développement Industriel (IRDI).

Blanchet, D., Buiron, L., Stauff, N., Kim, T., Taiwo, T., 2011. AEN-WPRS sodium fast reactor core definitions. Tech. rep., version 1.2–September 19th. CEA and Argonne National Laboratory.

Bonalumi, R., 1981. Rigorous homogenized diffusion theory parameters for neutrons. Nucl. Sci. Eng. 77 (2), 219–229.

Deniz, V., 1986. The theory of neutron leakage in reactor lattices. In: Yonen, R. (Ed.), CRC Handbook of Nuclear Reactor Calculations, vol. II. CRC Press, pp. 409–508.

Faure, B., 2016. Simulation des fuites neutroniques à l'aide d'un modèle B1 hétérogène pour des réacteurs à neutrons rapides et à eau légère (Master's thesis). École Polytechnique de Montréal.

Gelbard, E., 1983. Streaming in lattices. In: Lewins, J., Becker, M. (Eds.), Advances in Nuclear Science and Technology, vol. 15. Springer, US, pp. 223–400.

Hébert, A., 2009. Applied Reactor Physics. Presses internationales Polytechnique.

Hébert, A., Marleau, G., 1991. Generalization of the Stamm'ler method for the self-shielding of resonant isotopes in arbitrary geometries. Nucl. Sci. Eng. 108 (3), 230–239.

Kohler, P., 1975. A new definition of the cell diffusion coefficient. Nucl. Sci. Eng. (USA) 57 (4), 333–335.

Larsen, E., 1975. Neutron transport and diffusion in inhomogeneous media. I. J. Math. Phys. 16 (7), 1421–1427.

Leslie, D., 1962. The weighting of diffusion coefficients in cell calculations. J. Nucl. Eng. 16 (1), 1–11.

Petrovic, I., Benoist, P., 1997. Bn theory: advances and new models for neutron leakage calculation. Advances in Nuclear Science and Technology, Vol. 24. Springer, US, pp. 223–282.

Petrovic, I., Benoist, P., Marleau, G., 1996. A quasi-isotropic reflecting boundary condition for the TIBERE heterogeneous leakage model. Nucl. Sci. Eng. 122 (2), 151–166.

Rimpault, G., 1997. Physics documentation of ERANOS: the ECCO cell code. Rapport Technique RT/SPRC/LEPh, 97-001.

Rimpault, G., Vidal, J., Van-Rooijen, W., 2014. Neutron leakage treatment in reactor physics: consequences for predicting core characteristics. In: PHYSOR 2014 – The Role of Reactor Physics toward a Sustainable Future. Kyoto, Japan.

Smith, K.S., 2016. Nodal diffusion methods: understanding numerous unpublished details h0095 PHYSOR 2016 – Unifying Theory and Experiments in the 21st Century. Sun Valley, Idaho, U.S.A.

Van-Rooijen, W., Chiba, G., 2011. Diffusion coefficients for LMFBR cells calculated with MOC and Monte Carlo methods. Ann. Nucl. Energy 38 (1), 133–144.